remote sensing

MDPI

Technical Note

Wavelength Cut-Off Error of Spectral Density from MTF3 of SWIM Instrument Onboard CFOSAT: An Investigation from Buoy Data

Yuexin Luo [1,2,3], Ying Xu [2], Hao Qin [3,4] and Haoyu Jiang [1,2,4,*]

[1] College of Life Sciences and Oceanography, Shenzhen University, Shenzhen 518000, China
[2] Key Laboratory of Space Ocean Remote Sensing and Application, Ministry of Natural Resources, Beijing 100081, China
[3] College of Marine Science and Technology, China University of Geosciences, Wuhan 430074, China
[4] Shenzhen Research Institute, China University of Geosciences, Shenzhen 518000, China
* Correspondence: haoyujiang@szu.edu.cn

Abstract: The Surface Waves Investigation and Monitoring instrument (SWIM) provides the directional wave spectrum within the wavelength range of 23–500 m, corresponding to a frequency range of 0.056–0.26 Hz in deep water. This frequency range is narrower than the 0.02–0.485 Hz frequency range of buoys used to validate the SWIM nadir Significant Wave Height (SWH). The modulation transfer function used in the current version of the SWIM data product normalizes the energy of the wave spectrum using the nadir SWH. A discrepancy in the cut-off frequency/wavelength ranges between the nadir and off-nadir beams can lead to an overestimation of off-nadir cut-off SWHs and, consequently, the spectral densities of SWIM wave spectra. This study investigates such errors in SWHs due to the wavelength cut-off effect using buoy data. Results show that this wavelength cut-off error of SWH is small in general thanks to the high-frequency extension of the resolved frequency range. The corresponding high-frequency cut-off errors are systematic errors amenable to statistical correction, and the low-frequency cut-off error can be significant under swell-dominated conditions. By leveraging the properties of these errors, we successfully corrected the high-frequency cut-off SWH error using an artificial neural network and mitigated the low-frequency cut-off SWH error with the help of a numerical wave hindcast. These corrections significantly reduced the error in the estimated cut-off SWH, improving the bias, root-mean-square error, and correlation coefficient from 0.086 m, 0.111 m, and 0.9976 to 0 m, 0.039 m, and 0.9994, respectively.

Keywords: surface waves investigation and monitoring; China–France oceanography satellite; wave spectrum; significant wave height; modulation transfer function

check for updates

Citation: Luo, Y.; Xu, Y.; Qin, H.; Jiang, H. Wavelength Cut-Off Error of Spectral Density from MTF3 of SWIM Instrument Onboard CFOSAT: An Investigation from Buoy Data. *Remote Sens.* **2024**, *16*, 3092. https://doi.org/10.3390/rs16163092

Academic Editor: Vladimir N. Kudryavtsev

Received: 20 July 2024
Revised: 10 August 2024
Accepted: 21 August 2024
Published: 22 August 2024

Copyright: © 2024 by the authors. Licensee MDPI, Basel, Switzerland. This article is an open access article distributed under the terms and conditions of the Creative Commons Attribution (CC BY) license (https://creativecommons.org/licenses/by/4.0/).

1. Introduction

Wind-generated sea surface gravity waves (hereafter, referred to simply as waves) are one of the most common dynamic phenomena on the ocean surface. Observation of the waves plays a very important role across various domains including ocean engineering, marine disaster prevention and mitigation, and offshore structural design. Currently, operational wave observation relies primarily on two data sources—wave buoys and satellite remote sensing. For wave remote sensing, the two most commonly used types of remote sensors are satellite altimeters and Synthetic Aperture Radars (SARs), each with its own advantages and disadvantages. Altimeters can provide accurate observations of Significant Wave Height (SWH) [1–3] but are unable to capture wave spectra; SARs can obtain parts of the directional wave spectrum, but the so-called "azimuth cut-off" effect caused by the nonlinear imaging mechanism leads to the loss of high-frequency wave information in the wave spectrum [4]. The launching of the

China–France Oceanography SATellite (CFOSAT) in October 2018 opened new prospects for the observation of ocean waves.

The Surface Waves Investigation and Monitoring instrument (SWIM) onboard the CFOSAT is the world's first space-borne 'wave spectrometer'. SWIM is a six-beam rotating radar with small incidence angles (0–10°) operating at 13.575 GHz [5]. Its main task is to measure directional wave spectra in global open oceans. SWIM not only obtains wind speed and SWH information from the nadir beam like an altimeter but also obtains wave spectrum information from off-nadir beams with incidence angles of 6°–10°. At these low incidence angles, the normalized radar cross-section is sensitive to local slopes associated with long-wave tilts and is insensitive to wind-induced small-scale roughness as well as hydrodynamic modulations caused by the interaction between short and long waves. As a result, SWIM avoids the "azimuth cut-off" associated with SARs during wave spectrum measurements. It is capable of resolving waves with wavelengths of 70–500 m in the field-of-view direction [5]; however, according to the actual data files, the range of resolvable wavelengths is about 23–500 m. By combining unidirectional wave spectra from different directions through sensor rotation, SWIM produces a complete wave directional spectrum.

For retrieving wave spectral densities, the Modulation Transfer Function (MTF) currently used in the official SWIM data product is MTF3. This method directly normalizes the energy of the wave spectrum by using the energy derived from the nadir SWH as the total energy of the wave spectrum. Although MTF3 is more accurate in estimating the total energy of the wave spectrum compared to its predecessor, MTF1 [5], it introduces a potential wavelength cut-off error in the obtained wave spectrum. The wave spectrum measured by CFOSAT-SWIM has a wavelength range of 23–500 m, corresponding to a frequency range of 0.056–0.26 Hz in deep water. In contrast, the nadir SWH is an integral part of the spectral densities over a wider frequency range. The nadir SWH is often validated by in situ observations, such as the buoy data from the National Data Buoy Center (NDBC, e.g., [1–3]), and most NDBC buoys have a frequency range of 0.02–0.485 Hz. Therefore, the SWH corresponding to the SWIM spectrum should be considered as a cut-off SWH, and normalizing the energy of the cut-off wave spectrum with the SWH without the cut-off may result in an overestimation of the cut-off SWH and hence the spectral densities of the SWIM wave spectrum. This study aims to investigate the impact of SWIM's wavelength cut-off on wave spectral density using NDBC buoy data and to mitigate this impact to some extent.

2. Materials and Methods

2.1. NDBC Buoy Data

NDBC has a coastal-marine automated network comprising more than 100 buoys that measure wave spectra. Although these buoys can provide the first five Fourier coefficients of waves using their translational and pitch–roll data, only the energy spectra (i.e., the first Fourier coefficients) are used in this study because directional information is not considered. The data are available from the NDBC website (https://www.ndbc.noaa.gov/, accessed on 19 July 2024). We selected the data during the period from April 2019 to March 2023, applying the following criteria for buoy selection: (1) The buoys should have the data of the energy spectra covering the frequency range of 0.02–0.485 Hz; (2) The buoys should be more than 150 km from the coastlines, and the corresponding water depth should be more than 200 m so that the SWIM cut-off wavelengths can be easily converted to cut-off frequencies (0.056–0.26 Hz) using deep water dispersion relation. Following this screening process, 35 buoys meeting the criteria were retained, as depicted in Figure 1.

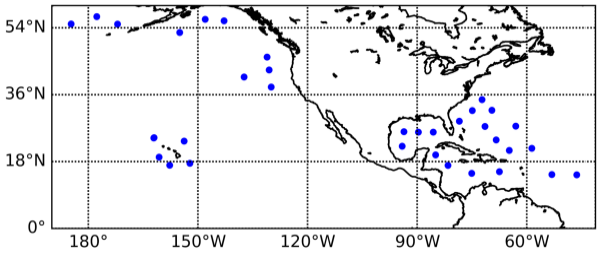


Figure 1. The location of the NDBC buoys used in this study.

2.2. Numerical Wave Model Hindcast

The wave spectrum data from the Integrated Ocean Waves for Geophysical and other Applications (IOWAGA) dataset are used as the axillary data to study the correction of the wavelength cut-off error in SWH. IOWAGA is a global hindcast wave field dataset generated using the WAVEWATCH III® model (version 6.07) [6] based on the source term package of ST4 [7] and forced by the global 10 m wind from the ERA5 dataset, surface currents from the CMEMS-Globcurrent, and ice concentrations from the IFREMER SSMI-derived daily product. Although the numerical wave model does not assimilate any observations, IOWAGA data show good agreement with both the in situ and altimeter observations [8]. The directional wave spectrum in this wave model is uniformly spaced across 24 directions and exponentially spaced across 36 frequencies ranging from 0.034 to 0.95 Hz with a 1.1 increment factor. The IOWAGA hindcast is run at a resolution of $0.5^\circ \times 3$ h, but a nested grid with a higher spatial resolution of $1/6^\circ$ is used in coastal regions. Full directional wave spectra and frequency spectra are available at more than 10,000 points along coastlines worldwide and at the locations of many moored buoys including those shown in Figure 1. More details of the dataset and the numerical wave model to generate this dataset can be found in [8].

2.3. Cut-Off SWH

Two types of SWHs are computed from the buoy wave spectra, the total SWH and the cut-off SWH. They are both computed using the following equations:

$$SWH = 4\sqrt{m_0} \tag{1}$$

$$m_n = \int_{f_{dn}}^{f_{up}} f^n E(f)\, \mathrm{d}f \tag{2}$$

where f is the frequency, m_n is the nth moment of the spectral density function $E(f)$, and f_{up} and f_{dn} are the high-frequency and low-frequency cut-offs of the measuring devices, respectively. For the total SWH, f_{up} and f_{dn} are set to 0.02 and 0.485 Hz, respectively, which are the cut-off frequencies for buoys. For the cut-off SWH, f_{up} and f_{dn} are set to 0.056 and 0.26 Hz, respectively, which are the cut-off frequencies for SWIM. The difference between the total and cut-off SWHs is then the wavelength cut-off error of SWH, which is equivalent to the error of spectral density due to wavelength cut-off when the spectral density is normalized by the total SWH. Hereafter, this wavelength/frequency cut-off error of SWH will be referred to simply as the cut-off SWH error, or cut-off error.

To test whether the cut-off error comes from the high-frequency or low-frequency part of the wave spectrum, we also compute the corresponding high-frequency and low-frequency cut-off SWHs where the integral frequency ranges are set to 0.02–0.26 Hz and 0.056–0.485 Hz, respectively. The high-frequency and low-frequency cut-off SWH errors are defined as the differences between the total SWH and the high-frequency and low-frequency cut-off SWHs, respectively.

2.4. Artificial Neural Network

An Artificial Neural Network (ANN) is used to correct the high-frequency cut-off SWH errors. An ANN can be thought of as a network of "neurons" organized into layers, including an input layer, one or more hidden layers, and an output layer. Upon receiving input and output data, the ANN establishes weighted connections between the input and output nodes through interconnected computing elements known as "neurons" situated in the hidden layers. The main advantage of an ANN is its theoretical ability to approximate any function with any number of input parameters, provided there are enough neurons and layers, making it a powerful non-linear fitting tool.

In Section 3, we demonstrate the nonlinear correlations of high-frequency cut-off errors with both wind speeds and SWHs, suggesting that the ANN might be well-suited for predicting the high-frequency cut-off error using wind speed and SWH as inputs. The buoy data are randomly divided into two groups, one for the training (10%) and the other for the validation (90%). Using only 10% of the data for training ensures the robustness of the statistical correction model. The ANN used here has an input layer with two neurons (wind speed and SWH), two hidden layers with 32 neurons each, and an output layer with one neuron. The activation function between different layers is the rectified linear unit (ReLU). The ANN is trained to minimize the Mean-Square Error (MSE) between the outputs and the targets (high-frequency cut-off SWH errors) using the Adam optimizer with a batch size of 512. The learning rate (initially set to 0.0002) decreased by 50% if the MSE of the training set did not decrease for two epochs, and the training process stopped when the MSE of the validation set did not decrease for ten epochs. It is also shown that having more hidden layers and hidden neurons does not significantly impact the model's performance.

3. Results

3.1. Evaluation of SWH Cut-Off Errors

Comparisons between the total and the three different cut-off SWHs, integrating over 0.056–0.26 Hz, 0.02–0.26 Hz, and 0.056–0.485 Hz, at all the buoys used in this study are shown as scatter plots in Figure 2a, Figure 2b, and Figure 2c, respectively. To evaluate the impact of the wavelength cut-off effect on the estimation of SWH, three error metrics are employed—bias, root-mean-square error (RMSE), and correlation coefficient (CC)—as follows:

$$Bias = \frac{1}{n}\sum_{i=1}^{n}(y_i - x_i) \tag{3}$$

$$RMSE = \sqrt{\frac{1}{n}\sum_{i=1}^{n}(y_i - x_i)^2} \tag{4}$$

$$R = \sum_{i=1}^{n}(y_i - \overline{y})(x_i - \overline{x}) \Big/ \left[\sqrt{\sum_{i=1}^{n}(y_i - \overline{y})^2}\sqrt{\sum_{i=1}^{n}(x_i - \overline{x})^2}\right] \tag{5}$$

where x and y denote the cut-off (including the high-frequency and low-frequency cut-off) SWHs and total SWHs, respectively, and the bars over them denote their mean values.

From Figure 2a, the first conclusion that can be drawn is that the wavelength cut-off does not significantly impact SWH estimation. The majority of the data closely align with the y = x line, with the bias, RMSE, and CC values of 0.086 m, 0.111 m, and 0.9976, respectively. Such a low value of RMSE is comparable with the SWH random noise observed by the NDBC buoys and altimeters [2], suggesting that the frequency/wavelength cut-off effect is not a major error source in SWIM's retrieval of wave spectra. This is probably one of the most important conclusions of this study, as it indicates that the cut-off effect will not significantly impact most applications of SWIM's wave spectral data. However, it is also noted that a large portion of the error comes from the systematic bias that can be corrected statistically, and there are still a few cases with significant cut-off errors, indicating that this issue warrants further investigation.

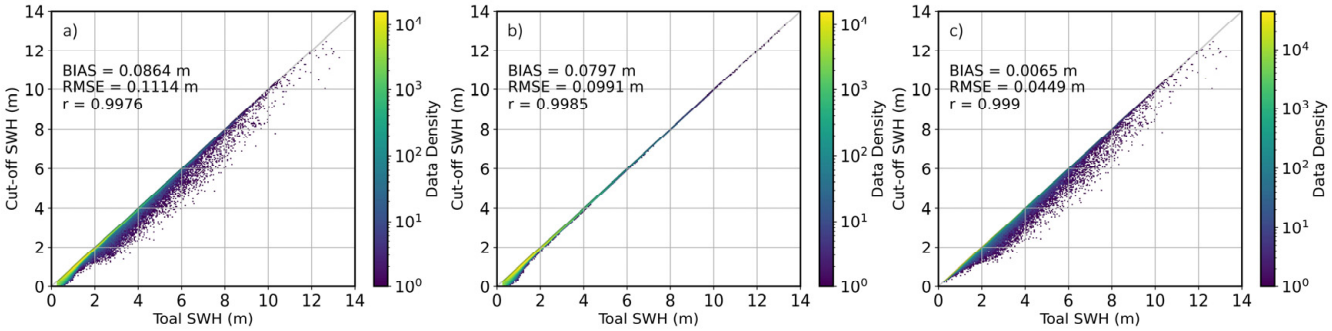


Figure 2. The scatter plot between the SWHs integrated from full buoy wave spectra (0.02–0.485 Hz) and from cut-off buoy wave spectra. The integral frequency range for the cut-off SWH is (**a**) 0.056–0.26 Hz, (**b**) 0.02–0.26 Hz (high-frequency cut-off SWH), and (**c**) 0.056–0.485 Hz.

A closer examination of the high-frequency and low-frequency cut-off SWHs reveals an interesting pattern, where most of the errors stem from the cut-off of the high-frequency tails of the spectra (Figure 2b), while the few cases with large errors are due to the low-frequency cut-off (Figure 2c). Although both the bias and RMSE in Figure 2b are significantly larger than those in Figure 2c, and the CC is lower in Figure 2b than in Figure 2c, the scatter plot in Figure 2b appears to show better agreement than Figure 2c, as it is much less scattered. This suggests that a large proportion of the errors in Figure 2b originates from the correctable systematic bias between the total and cut-off SWHs. Despite the more scattered appearance of Figure 2c, it is important to highlight that these "outliers" represent a very small fraction of the dataset and have only a minimal impact on the overall error metrics, where only 1.2% of the data has residual >0.1 m in Figure 2c, and this value decreases to 0.5% for residual exceeding 0.25 m.

To further investigate the dependence of these errors on other variables, the cut-off errors of SWH as functions of total SWH and wind speed are shown in Figure 3. A weak yet statistically significant correlation (CC $\approx$ 0.22) is found between the low-frequency cut-off errors and SWHs, but no clear pattern is found in Figure 3a. Similarly, in Figure 3b, the correlation between the low-frequency cut-off errors and wind speeds is not statistically significant. In contrast, the high-frequency cut-off errors exhibit stronger correlations with both wind speeds and SWHs, with CCs of 0.33 and -0.33, respectively. Although the CCs of ± 0.33 are still low (but statistically significant and higher than the CC in Figure 3a), clear patterns can be observed in Figure 3c,d, where high-frequency cut-off errors increase with the increase in wind speed and with the decrease in SWH. These dependencies might be helpful for the correction of high-frequency cut-off errors.

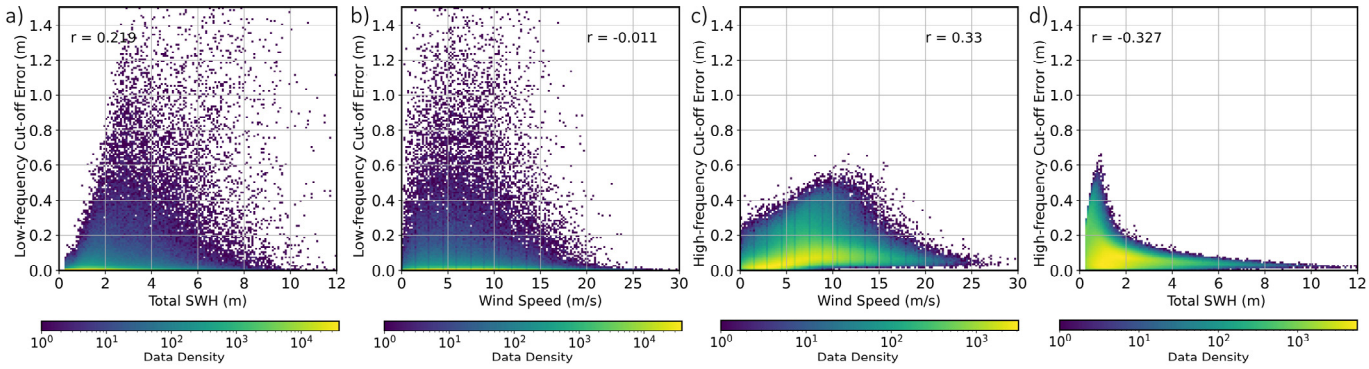


Figure 3. Wavelength cut-off error of SWH as functions of total SWH and wind speed. (**a**,**b**) Low-frequency cut-off errors as a function of SWH and wind speed, respectively. (**c**,**d**) The same as subplots a and b but for high-frequency cut-off errors.

3.2. Correction of High-Frequency Cut-Off Errors of SWH

The high-frequency cut-off errors appear to be systematic, with their magnitudes significantly correlated to both wind speeds and SWHs, as shown in Figure 3c,d. From a physical point of view, previous studies have shown that these high-frequency tails of the wave spectrum, known as the "equilibrium range", respond rapidly to local wind, especially in the open ocean [9]. Additionally, it has been shown that the shape of the "equilibrium range" can be utilized to estimate wind speed [10,11]. These correlations suggest that the correction of high-frequency cut-off errors is promising.

Since wind speed is available, the high-frequency tail can be computed using the f^{-4} relation (the impact of the saturation range f^{-5} on the SWH is small):

$$E(f) = \frac{4\beta I u_* g}{(2\pi)^3} f^{-4} \tag{6}$$

where β is an empirical constant, and I was introduced to allow for enhanced tail energy levels for different directional spread. If one assumes that I is constant and the wind profile is known (e.g., the log profile), then the cut-off energy can be estimated using Equation (6). However, this semi-analytical method might involve relatively large errors, as shown by previous attempts to estimate wind speed using wave spectra [10,11].

Given the availability of wind speed and total SWH data from SWIM, a model was developed to correct high-frequency cut-off SWH errors, employing wind speed and SWH as inputs. As depicted in Figure 3c,d, the correlations of high-frequency cut-off errors with both wind speed and SWHs are nonlinear. Therefore, we try to use an ANN to conduct this correction simply because ANN can handle the problem of multivariate nonlinear fitting well and is widely used in the statistical correction of systematic errors in wave remote sensing (e.g., [2,12]).

After applying the ANN-based correction, on which more information is available in Section 2.4, the comparison between the corrected high-frequency cut-off SWHs and the buoy-derived high-frequency cut-off SWHs (for the validation set) is shown in Figure 4a. Compared to the results in Figure 2b, the bias is eliminated, the RMSE decreases from 0.099 m to 0.035 m, and the CC increases from 0.9985 to 0.9994, showing that this statistical method can effectively correct the high-frequency cut-off error. After the correction, the most significant errors (although they are small) are observed under conditions of low SWHs, primarily because even a very small error in spectral density can result in a relatively large error in SWH when SWHs are low.

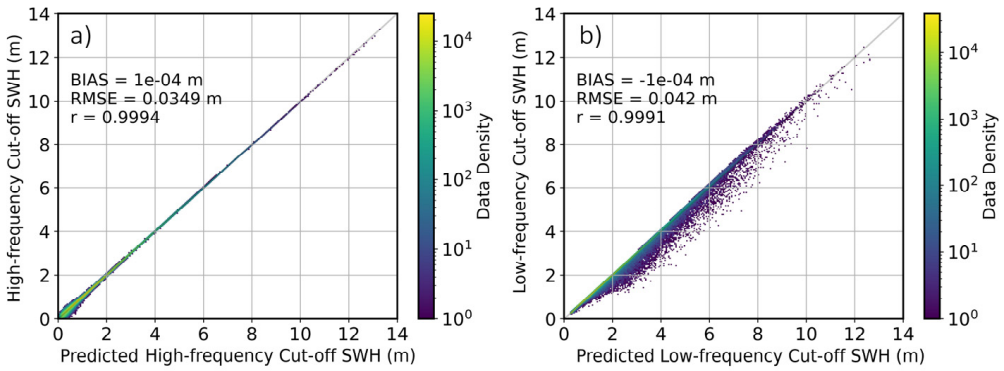


Figure 4. (**a**) Comparison between the high-frequency cut-off SWHs (0.02–0.26 Hz) from ANN correction and from the original buoy data. (**b**) The same as (**a**) but for low-frequency cut-off SWHs (0.056–0.485 Hz).

3.3. Correction of Low-Frequency Cut-Off Errors of SWH

Compared to the high-frequency errors that are correlated to local winds and SWHs, the correction of low-frequency errors is more challenging. As previously discussed, the

low-frequency cut-off error of SWH comes from long swells generated by the westerlies and propagated into the buoy locations. These long swells are not directly correlated to any local variables from a physical standpoint because they are simply remote signals passing through the given area. Consequently, correcting the low-frequency cut-off error of SWH through statistical methods is unlikely to be effective. We attempted to apply the aforementioned ANN for this correction, but the results in Figure 4b aligned with our expectations—the statistical correction was ineffective for correcting the low-frequency cut-off error. The ANN marginally reduced the RMSE from 0.045 m to 0.042 m and increased the CC from 0.9990 to 0.9991, but the scattering of data in Figure 4b remained almost unchanged compared to Figure 2c.

Given the ineffectiveness of statistical methods in correcting low-frequency cut-off errors, such an error might only be corrected using the dynamic way, i.e., with the help of a numerical wave model forecast or hindcast.

For spectral densities at frequencies lower than 0.056 Hz, the difference between the results from wave forecasts and hindcasts is small because the energy at such low frequencies is dependent only on the historical and remote wind field [13]. In this study, we tried to use the omnidirectional wave spectra from the IOWAGA dataset to correct the low-frequency cut-off errors. Although the lowest frequency resolved by the IOWAGA dataset is 0.034 Hz, which is higher than that which has been resolved by the buoy (0.02 Hz), it can be seen from Figure 2b that there is almost no wave energy for frequencies lower than 0.034 Hz in the buoy data, even for swell-dominated cases. Therefore, the cut-off frequency of the model is not an issue for the energy correction. Although contemporary numerical models still face challenges in accurately modeling swells that propagate over large distances [4,14,15], we believe that they can at least reflect a part of the cut-off low-frequency error.

Figure 5a shows the comparison of the low-frequency cut-off errors computed from the buoy data and the corresponding model data. Although the agreement between these two sets of data might not seem satisfactory at first glance, it is noted that the CC between the two error values exceeds 0.8, which can be regarded as a high value. This means that the low-frequency cut-off error can be, at least, partly reflected and corrected using a numerical wave model. The error correction process is carried out as follows: First, the modeled proportions of cut-off energy (energy below 0.056 Hz) are linearly regressed against the buoy-observed proportions of cut-off energy to reduce the systematic error of energy between the model and buoy in low frequencies. Then, the low-frequency cut-off error δ_{LF} is estimated as follows:

$$\delta_{LF} = \sqrt{SWH^2 \times p} \tag{7}$$

where p is the modeled proportions of cut-off energy after the correction in the first step. This correction method yields slightly better results than a direct correction using the model-estimated low-frequency cut-off error (also adjusted by linear regression). Figure 5b shows the comparison between the high-frequency cut-off SWHs (0.056–0.45 Hz) after this correction and from the original buoy data. Compared to the results in Figure 4b, most outliers with large errors are effectively eliminated, the RMSE decreases from 0.042 m to 0.020 m, and the CC increases from 0.9991 to 0.9998. Finally, combining the corrections for both high-frequency and low-frequency cut-off errors, the comparison between the predicted and buoy-measured cut-off SWH is shown in Figure 5c. It is evident that the potential wavelength cut-off error of SWH is significantly reduced, and it will be more reasonable for the MTF of SWIM to use the estimated cut-off SWH to normalize the wave spectra.

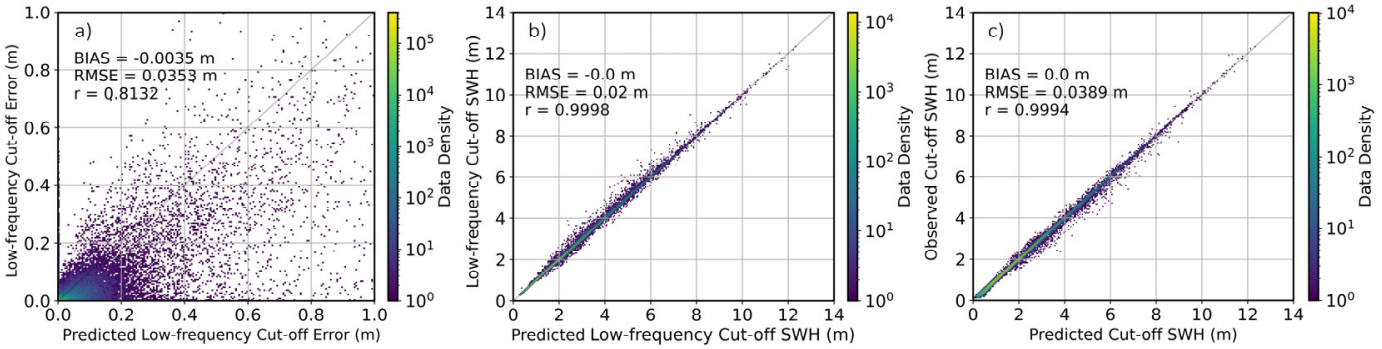


Figure 5. (**a**) The scatter plot between the low-frequency cut-off errors of SWH derived from buoys and those from IOWAGA. (**b**) The scatter plot between the low-frequency cut-off SWHs (0.056–0.485 Hz) after correction using the numerical wave model and the original buoy data. (**c**) The scatter plot between the cut-off SWHs (0.056–0.26 Hz) from direct buoy observations and those from the correction method presented in this study.

4. Discussion

To better understand the cut-off error of SWH, Figure 6a shows four mean buoy spectra for different SWHs. The figure shows that a small portion of wave energy is cut off at both high and low frequencies. When SWHs are high (e.g., the red curve), the cut-off energy is only a very small proportion of the total energy, especially in the high-frequency range, resulting in a small error in SWH estimation. However, when the SWHs are low (e.g., the orange curve), the proportion of high-frequency cut-off energy becomes large, resulting in SWHs which are in agreement with Figures 2b and 3d, where the high-frequency cut-off errors are negatively correlated to SWH. This can also be regarded as the physical basis for using the total SWH as the input of ANN for correcting high-frequency cut-off errors.

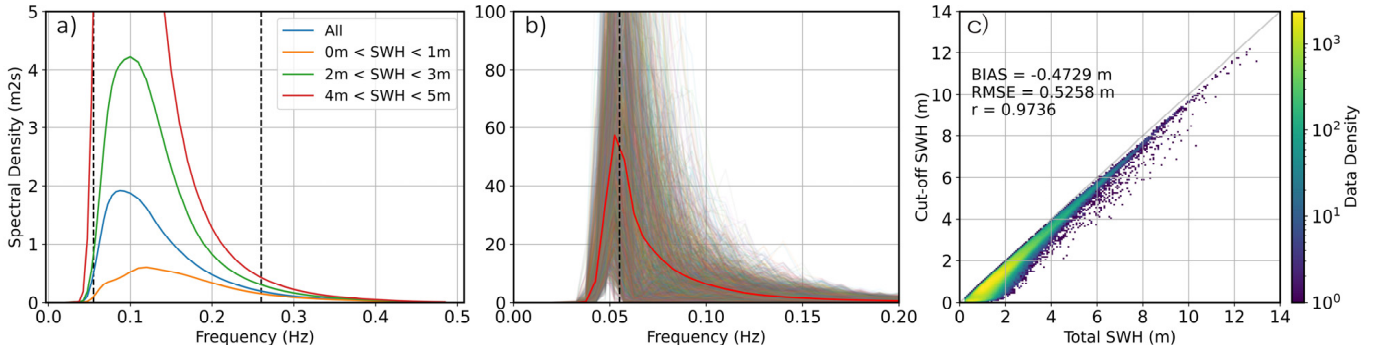


Figure 6. (**a**) Mean buoy spectra for the entire sample (blue) and for different SWH ranges (other colors) with vertical dashed line indicates the cut-off frequencies. (**b**) Buoy spectra for cases with cut-off errors exceed 0.5 m, where the red curve indicates their mean spectrum. (**c**) The same as Figure 2a, but using the nominal cut-off range of SWIM, 70 to 500 m.

For SWH < 3 m, the low-frequency cut-off energy remains lower than the high-frequency cut-off energy, and its contribution to the total energy diminishes as SWH increases. This explains why the low-frequency cut-off effect is negligible in most cases, regardless of whether the SWH is low or high.

Another noteworthy feature in Figure 6a is that the wavelength cut-off error of SWH, particularly the high-frequency cut-off error, would be significant if the resolved wavelength ranged only from 70 to 500 m (0.0565 to 0.15 Hz). This is because spectral densities at frequencies of above 0.15 Hz contribute significantly to the total energy in cases with SWHs at below 3 m. The comparison between the total and cut-off SWHs using the nominal cut-off range of SWIM (70 to 500 m), as shown in Figure 6c, supports the above inference. Both the bias and RMSE are about four times greater than those in Figure 2a, with errors

being particularly significant in low-SWH cases. However, thanks to the extension of the resolved frequency range, the impact of high-frequency cut-off error is greatly reduced.

Figure 6b shows the mean spectrum for instances with cut-off errors exceeding 0.5 m (this threshold is arbitrarily selected, yet it was checked that varying it from 0.2 to 0.8 m has negligible impact on the result). For the cases of large cut-off error, the mean spectrum exhibits a distinct profile, characterized by the peak frequency being lower than the cut-off frequency, indicating that all significant cut-off errors originate from the cut-off in low frequencies. In these instances, the spectra are dominated by long swells that probably cannot be fully resolved by SWIM, and this will lead to a significant overestimation of the SWIM spectral density by MTF3.

Further examination of cases with low-frequency cut-off errors in excess of 0.2 m revealed that more than 95% of them have a peak frequency lower than 0.07 Hz (equivalent to a peak period of ~14 s). Most waves with such low peak frequencies are swells generated by remote wind (especially extra-tropical storms in the westerlies). Although cases of relatively large low-frequency cut-off errors in SWHs make up only a small fraction of the buoy dataset, this cut-off error has a large impact on the observation and study of long ocean swells propagating across the ocean. When using SWIM data to track very long swells, it is important to account for this low-frequency cut-off effect, as the spectral densities in the current version of the data product might be significantly overestimated for such long swell events.

5. Conclusions

The SWIM is capable of resolving the directional wave spectrum within a wavelength range of 23–500 m, which corresponds to a frequency range of 0.056–0.26 Hz in deep water. Meanwhile, the SWHs obtained by the nadir beam of SWIM, which are used to normalize the off-nadir SWIM wave spectra in MTF3, are validated using the buoy-observed SWHs calculated from the spectral energy within a broader frequency range of 0.02 Hz to 0.485 Hz. This mismatch in frequency ranges can potentially lead to an overestimation of the SWIM spectral densities. This study investigated this frequency/wavelength cut-off error using the wave spectra from buoys. The comparison of SWHs before and after the frequency cut-off revealed that the wavelength cut-off error is generally small. However, the high-frequency cut-off can cause a systematic bias in SWH of nearly 0.1 m, while the low-frequency cut-off can lead to significant errors under conditions of long swells. These cut-off errors in wave energy will be proportionally distributed across the SWIM wave spectra, leading to a proportional overestimation of the energy in each wave spectrum.

Understanding the nature of these errors, it was found that the high-frequency cut-off error can be statistically corrected using wind speed and SWH information. This is because the high-frequency cut-off error arises from the tails of the wave spectra that respond rapidly to local wind, and a proportion of the tail energy within the entire spectrum decreases with increasing SWH. An ANN, using wind speed and SWH as inputs, was employed and successfully corrected the high-frequency cut-off error.

In contrast, the low-frequency cut-off error, which comes from swells generated elsewhere, could not be effectively corrected using statistical methods. Fortunately, contemporary numerical wave models can provide some information on these long swells. Thus, the low-frequency cut-off error of SWH is partially corrected with the help of the output of a numerical wave model. Although it is understood that access to modeled wave spectra is not universally available across the global ocean, we failed to figure out a better way to correct low-frequency cut-off errors. Thus, it is also recommended that the future SWIM data product incorporates the along-track modeled wave spectra.

Following these corrections, the error in the estimated cut-off SWH was substantially reduced. The bias, RMSE, and CC improved from 0.086 m, 0.111 m, and 0.9976 to 0 m, 0.039 m, and 0.9994, respectively. Although this wavelength/frequency cut-off error may be considered second-order compared to other known error sources such as speckle noise and parasitic peaks, its significance should not be overlooked, particularly in cases involving

low SWHs and long swells. Given that this error can be substantially corrected using our method, we hope that future versions of the SWIM data product will incorporate this correction or simply further extend the frequency range of the spectrum.

Author Contributions: Conceptualization, H.J.; methodology, H.J. and Y.L.; software, H.J. and Y.L.; validation, H.J.; formal analysis, H.J. and Y.L.; investigation, H.J. and Y.L.; resources, H.J. and Y.X.; data curation, Y.L. and H.J.; writing—original draft preparation, Y.L. and H.J.; writing—review and editing, H.Q. and Y.X.; visualization, H.J.; supervision, H.J.; project administration, Y.X.; funding acquisition, H.J. All authors have read and agreed to the published version of the manuscript.

Funding: This research was funded partly by the National Key Research and Development Program of China, grant number 2022YFC3104900-2022YFC3104905, partly by the National Natural Science Foundation of China, grant number 42376172, partly by the Key Laboratory of Space Ocean Remote Sensing and Application, MNR, grant number 2023CFO008, and partly by the Guangdong Basic and Applied Basic Research Foundation, grant number, 2022A1515240069/2024A1515012032/2023A1515240047.

Data Availability Statement: The NDBC buoy data are available from NDBC website (ASCII, https://www.ndbc.noaa.gov/, accessed on 19 July 2024). The IOWAGA dataset is available from (Alday et al., 2021) and can be downloaded from the official website of LOPS, IFREMER (https://www.umr-lops.fr/Donnees/Vagues, accessed on 19 July 2024).

Conflicts of Interest: The authors declare no conflicts of interest.

References

1. Dodet, G.; Piolle, J.-F.; Quilfen, Y.; Abdalla, S.; Accensi, M.; Ardhuin, F.; Ash, E.; Bidlot, J.-R.; Gommenginger, C.; Marechal, G.; et al. The Sea State CCI dataset v1: Towards a sea state climate data record based on satellite observations. *Earth Syst. Sci. Data* **2020**, *12*, 1929–1951. [CrossRef]
2. Jiang, H. Random, Environmental, and representativeness errors in ocean remote sensing versus in situ data: An example of wave heights from altimeters. *IEEE Trans. Geosci. Remote Sens.* **2023**, *61*, 4205613. [CrossRef]
3. Ribal, A.; Young, I.R. 33 years of globally calibrated wave height and wind speed data based on altimeter observations. *Sci. Data* **2019**, *6*, 77. [CrossRef] [PubMed]
4. Ardhuin, F.; Chapron, B.; Collard, F. Observation of swell dissipation across oceans. *Geophys. Res. Lett.* **2009**, *36*, L06607. [CrossRef]
5. Hauser, D.; Tourain, C.; Hermozo, L.; Alraddawi, D.; Aouf, L.; Chapron, B.; Dalphinet, A.; Delaye, L.; Dalila, M.; Dormy, E.; et al. New Observations from the SWIM Radar On-Board CFOSAT: Instrument Validation and Ocean Wave Measurement Assessment. *IEEE Trans. Geosci. Remote Sens.* **2021**, *59*, 5–26. [CrossRef]
6. The WAVEWATCH III® Development Group. User Manual and System Documentation of WAVEWATCH III® Version 5.16. Tech. Note, NOAA/NWS/NCEP/MMAB, College Park. MD, USA. 2016. Available online: https://polar.ncep.noaa.gov/waves/wavewatch/manual.v5.16.pdf (accessed on 19 July 2024).
7. Ardhuin, F.; Rogers, E.; Babanin, A.V.; Filipot, J.-F.; Magne, R.; Roland, A.; van der Westhuysen, A.; Queffeulou, P.; Lefevre, J.-M.; Aouf, L.; et al. Semiempirical Dissipation Source Functions for Ocean Waves. Part I: Definition, Calibration, and Validation. *J. Phys. Oceanogr.* **2010**, *40*, 1917–1941. [CrossRef]
8. Alday, M.; Accensi, M.; Ardhuin, F.; Dodet, G. A global wave parameter database for geophysical applications. Part 3: Improved forcing and spectral resolution. *Ocean Model.* **2021**, *166*, 101848. [CrossRef]
9. Phillips, O.M. Spectral and statistical properties of the equilibrium range in wind-generated gravity waves. *J. Fluid Mech.* **1985**, *156*, 505–531. [CrossRef]
10. Voermans, J.J.; Smit, P.B.; Janssen, T.T.; Babanin, A. V Estimating Wind Speed and Direction Using Wave Spectra. *J. Geophys. Res. Ocean.* **2020**, *125*, e2019JC015717. [CrossRef]
11. Jiang, H. Wind speed and direction estimation from wave spectra using deep learning. *Atmos. Meas. Tech.* **2022**, *15*, 1–9. [CrossRef]
12. Jiang, H.; Song, Y.; Mironov, A.; Yang, Z.; Xu, Y.; Liu, J. Accurate mean wave period from SWIM instrument on-board CFOSAT. *Remote Sens. Environ.* **2022**, *280*, 113149. [CrossRef]
13. Jiang, H.; Mu, L. Wave climate from spectra and its connections with local and remote wind climate. *J. Phys. Oceanogr.* **2019**, *49*, 543–559. [CrossRef]

14. Jiang, H.; Stopa, J.E.; Wang, H.; Husson, R.; Mouche, A.; Chapron, B.; Chen, G. Tracking the attenuation and nonbreaking dissipation of swells using altimeters. *J. Geophys. Res. Ocean.* **2016**, *121*, 1446–1458. [CrossRef]
15. Jiang, H.; Babanin, A.V.; Chen, G. Event-based validation of swell arrival time. *J. Phys. Oceanogr.* **2016**, *46*, 3563–3569. [CrossRef]

Disclaimer/Publisher's Note: The statements, opinions and data contained in all publications are solely those of the individual author(s) and contributor(s) and not of MDPI and/or the editor(s). MDPI and/or the editor(s) disclaim responsibility for any injury to people or property resulting from any ideas, methods, instructions or products referred to in the content.